A&A 665, A151 (2022)
https://doi.org/10.1051/0004-6361/202243584

Astronomy & Astrophysics

The miniJPAS survey: White dwarf science with 56 optical filters

C. López-Sanjuan[1], P.-E. Tremblay[2], A. Ederoclite[3], H. Vázquez Ramió[1], A. J. Cenarro[1], A. Marín-Franch[1], J. Varela[1], S. Akras[4], M. A. Guerrero[5], F. M. Jiménez-Esteban[6,7], R. Lopes de Oliveira[8,9], A. L. Chies-Santos[10,11], J. A. Fernández-Ontiveros[3], R. Abramo[12], J. Alcaniz[9], N. Benítez[5], S. Bonoli[13,14,3], S. Carneiro[15], D. Cristóbal-Hornillos[3], R. A. Dupke[9,16,17], C. Mendes de Oliveira[18], M. Moles[3], L. Sodré Jr.[18], and K. Taylor[19]

[1] Centro de Estudios de Física del Cosmos de Aragón (CEFCA), Unidad Asociada al CSIC, Plaza San Juan 1, 44001 Teruel, Spain
e-mail: clsj@cefca.es
[2] Department of Physics, University of Warwick, Coventry CV4 7AL, UK
[3] Centro de Estudios de Física del Cosmos de Aragón (CEFCA), Plaza San Juan 1, 44001 Teruel, Spain
[4] Institute for Astronomy, Astrophysics, Space Applications and Remote Sensing, National Observatory of Athens, Penteli 15236, Greece
[5] Instituto de Astrofísica de Andalucía, IAA-CSIC, Glorieta de la Astronomía S/N, 18008 Granada, Spain
[6] Centro de Astrobiología (CSIC-INTA), ESAC Campus, Camino Bajo del Castillo S/N, 28692 Villanueva de la Cañada, Spain
[7] Spanish Virtual Observatory, 28692 Villanueva de la Cañada, Spain
[8] Departamento de Física, Universidade Federal de Sergipe, Av. Marechal Rondon S/N, 49100-000 São Cristóvão, Brazil
[9] Observatório Nacional – MCTI (ON), Rua Gal. José Cristino 77, São Cristóvão, 20921-400 Rio de Janeiro, Brazil
[10] Instituto de Física, Universidade Federal do Rio Grande do Sul (UFRGS), Av. Bento Gonçalves, 9500 Porto Alegre, RS, Brazil
[11] Shanghai Astronomical Observatory, Chinese Academy of Sciences, 80 Nandan Rd., Shanghai 200030, PR China
[12] Instituto de Física, Universidade de São Paulo, Rua do Matão 1371, 05508-090 São Paulo, Brazil
[13] Donostia International Physics Centre (DIPC), Paseo Manuel de Lardizabal 4, 20018 Donostia-San Sebastián, Spain
[14] IKERBASQUE, Basque Foundation for Science, 48013 Bilbao, Spain
[15] Instituto de Física, Universidade Federal da Bahia, 40210-340 Salvador, BA, Brazil
[16] University of Michigan, Department of Astronomy, 1085 South University Ave., Ann Arbor, MI 48109, USA
[17] University of Alabama, Department of Physics and Astronomy, Gallalee Hall, Tuscaloosa, AL 35401, USA
[18] Instituto de Astronomia, Geofísica e Ciências Atmosféricas, Universidade de São Paulo, 05508-090 São Paulo, Brazil
[19] Instruments4, 4121 Pembury Place, La Canada Flintridge, CA 91011, USA

Received 18 March 2022 / Accepted 10 July 2022

ABSTRACT

Aims. We analyze the white dwarf population in miniJPAS, the first square degree observed with 56 medium-band, 145 Å in width optical filters by the Javalambre Physics of the accelerating Universe Astrophysical Survey (J-PAS), to provide a data-based forecast for the white dwarf science with low-resolution ($R \sim 50$) photo-spectra.
Methods. We define the sample of the bluest point-like sources in miniJPAS with $r < 21.5$ mag, a point-like probability larger than 0.5, $(u - r) < 0.80$ mag, and $(g - i) < 0.25$ mag. This sample comprises 33 sources with spectroscopic information: 11 white dwarfs and 22 quasi-stellar objects (QSOs). We estimate the effective temperature ($T_{\rm eff}$), the surface gravity, and the composition of the white dwarf population by a Bayesian fitting to the observed photo-spectra.
Results. The miniJPAS data are sensitive to the Balmer series and the presence of polluting metals. Our results, combined with those from the Javalambre Photometric Local Universe Survey (J-PLUS) which has a lower spectral resolution but has already observed thousands of white dwarfs, suggest that J-PAS photometry would permit – down to $r \sim 21.5$ mag and at least for sources with $7000 < T_{\rm eff} < 22\,000$ K – both the classification of the observed white dwarfs into H-dominated and He-dominated with 99% confidence and the detection of calcium absorption for equivalent widths larger than 15 Å. The effective temperature is estimated with a 2% uncertainty, which is close to the 1% from spectroscopy. A precise estimation of the surface gravity depends on the available parallax information. In addition, the white dwarf population at $T_{\rm eff} > 7000$ K can be segregated from the bluest extragalactic QSOs, providing a clean sample based on optical photometry alone.
Conclusions. The J-PAS low-resolution photo-spectra would produce precise effective temperatures and atmospheric compositions for white dwarfs, complementing the data from *Gaia*. J-PAS will also detect and characterize new white dwarfs beyond the *Gaia* magnitude limit, providing faint candidates for spectroscopic follow-up.

Key words. white dwarfs – surveys – techniques: photometric – methods: statistical

1. Introduction

White dwarfs are the degenerate remnant of stars with masses lower than 8−10 $M_\odot$ and the endpoint of the stellar evolution for more than 97% of stars (e.g., Ibeling & Heger 2013; Doherty et al. 2015, and references therein). This makes them an essential tool to disentangle the star formation history of the Milky Way, to study the late phases of stellar evolution, and to understand the physics of condensed matter.

White dwarfs can be selected from the general stellar population thanks to their location in the Hertzsprung–Russell (H–R) diagram; they are typically ten magnitudes fainter than main sequence stars of the same effective temperature. The pioneering analysis by Russell (1914) and Hertzsprung (1915)

shows only one faint A-type star, 40 Eri B, with the inclusion of Sirius B (Adams 1915) and van Maanen 2 (van Maanen 1917, 1920) in the lower left-hand corner of the H–R diagram by the end of that decade. The initial doubts about the high density derived for these objects were clarified during the next years thanks to the estimation of the gravitational redshift of Sirius B (Adams 1925) and the proposal of electron degeneracy pressure as a counterbalance for the gravitational collapse caused by such condensed matter (Fowler 1926). Once established as an astrophysical object (see Holberg 2009, for a detailed review), the systematic analysis of the white dwarf population began.

The use of the H–R diagram to search for new white dwarfs was limited by the difficulties in the estimation of precise parallaxes, which are needed to obtain the luminosity of the objects. Because of this, the definition of photometric white dwarf catalogs was mainly based on the search of ultraviolet-excess objects – such as the Palomar–Green (PG) catalog (Green et al. 1986), the Kiso survey (KUV, Noguchi et al. 1980; Kondo et al. 1984), or the Kitt Peak–Downes (KPD) survey (Downes 1986) – and using reduced proper motions (e.g., Luyten 1979; Harris et al. 2006; Rowell & Hambly 2011; Gentile Fusillo et al. 2015; Munn et al. 2017). The spectroscopic follow-up of these photometric catalogs revealed a diversity of white dwarf atmospheric compositions (Sion et al. 1983; Wesemael et al. 1993), with sources presenting hydrogen lines (DA type), He II lines (DO), He I lines (DB), metal lines (DZ), featureless spectra (DC), among others. By the end of the XXth century, about ∼3000 white dwarfs with spectroscopic information and only ∼300 with precise parallax measurements were cataloged (McCook & Sion 1999).

This difference further increased by one order of magnitude mainly thanks to the spectroscopy from the Sloan Digital Sky Survey (SDSS, York et al. 2000). During almost 20 years of observations, the different SDSS data releases increased the number of white dwarfs with spectroscopic information to above 20 000 (Kleinman et al. 2004; Eisenstein et al. 2006; Kepler et al. 2015, 2016, 2019). At the same time, the absolute number of white dwarfs with precise parallaxes did not increase significantly (e.g., Leggett et al. 2018).

The high-quality data from the *Gaia* mission (Gaia Collaboration 2016) changed the situation. Thanks to *Gaia* parallaxes and photometry, the efficient use of the H–R diagram to unveil the white dwarf population became feasible, with more that 350 000 candidates reported so far (Gentile Fusillo et al. 2019, 2021). It also permits the definition of high-confidence volume-limited white dwarf samples (Hollands et al. 2018; Jiménez-Esteban et al. 2018; Kilic et al. 2020; McCleery et al. 2020; Gaia Collaboration 2021b).

Gathering spectral information of the *Gaia*-based samples is a key observational goal to advance white dwarf science in the forthcoming years. Current and planned multi-object spectroscopic surveys, such as the SDSS-V Milky Way mapper (Kollmeier et al. 2017), the Large Sky Area Multi-Object Fiber Spectroscopic Telescope (LAMOST, Cui et al. 2012), the *William Herschel* Telescope Enhanced Area Velocity Explorer (WEAVE, Dalton et al. 2012), the Dark Energy Spectroscopic Instrument (DESI, Allende Prieto et al. 2020), and the 4-m Multi-Object Spectrograph Telescope (4MOST, Chiappini et al. 2019), are going to observe a hundred thousand spectra of white dwarfs. In addition, the low-resolution ($R \sim 30$–90) blue photometer/red photometer (BP/RP) spectra from *Gaia* DR3 (De Angeli et al. 2022; Montegriffo et al. 2022) and beyond provide valuable information for the white dwarf population (Carrasco et al. 2014; Gaia Collaboration 2022).

The exploitation of the spectroscopic data above can be enhanced by the photometry from the Javalambre Physics of the accelerating Universe Astrophysical Survey[1] (J-PAS, Benítez et al. 2014), comprising 56 optical passbands with a full width at half maximum (FWHM) of FWHM $\approx$ 145 Å which provide low-resolution photo-spectra ($R \sim 50$) over several thousand square degrees in the northern sky. J-PAS already released its first square degree in the Extended Groth Strip (EGS) area, named miniJPAS (Bonoli et al. 2021), providing a unique data set to test the capabilities of low-resolution spectral information for white dwarf science. Furthermore, and given the comparable spectral resolution, the miniJPAS analysis also yields a data-based forecast for *Gaia* BP/RP spectra. We aim to study the white dwarf population in miniJPAS with 56 optical filters, forecasting its capabilities in the estimation of the effective temperature ($T_{\rm eff}$), the surface gravity ($\log g$), the atmospheric composition (hydrogen versus helium dominated), the detection of polluting metals, and the discrimination of extragalactic quasi-stellar objects (QSOs) with similar broadband colors.

This paper is organized as follows. We present the miniJPAS data and the bluest point-like sample in Sect. 2. The Bayesian analysis of the sources is detailed in Sect. 3. The results and the comparison with spectroscopy are described in Sect. 4. The separation between white dwarfs and QSOs is explored in Sect. 5. Finally, Sect. 6 is devoted to the discussion, the synergies with *Gaia*, and the conclusions. Magnitudes are expressed in the AB system (Oke & Gunn 1983).

2. Data and sample definition

2.1. MiniJPAS photometric data

The miniJPAS was carried out at the Observatorio Astrofísico de Javalambre (OAJ, Cenarro et al. 2014), located at the Pico del Buitre in the Sierra de Javalambre, Teruel (Spain). The data were acquired with the 2.5 m Javalambre Survey Telescope (JST250) and the JPAS-Pathfinder (JPF) camera, which was the first scientific instrument installed at JST250 before the arrival of JPCam (Taylor et al. 2014; Marín-Franch et al. 2017). The JPF instrument is a single 9200 × 9200 CCD located at the center of the JST250 field of view (FoV) with a pixel scale of 0.23 arcsec pixel^{-1}, providing an effective FoV of 0.27 deg^2.

The J-PAS filter system comprises 54 filters with a FWHM of 145 Å that are spaced every ≈100 Å from 3800 Å to 9100 Å. They are complemented with two broader filters at the blue and red end of the optical range, with an effective wavelength of 3479 Å (u, FWHM = 509 Å) and 9316 Å ($J1007$, FWHM = 635 Å), respectively. This filter system was optimized for delivering a low-resolution ($R \sim 50$) photo-spectrum of each surveyed pixel. The technical description and characterization of the J-PAS filters are presented in Marín-Franch et al. (2012). Detailed information of the filters as well as their transmission curves can be found at the Spanish Virtual Observatory Filter Profile Service[2]. In addition, miniJPAS includes four SDSS-like broadband filters, named $u_J gri$.

The miniJPAS observations comprise four JPF pointings in the EGS along a strip aligned at 45 deg with respect to north at (RA, Dec) = (215, +53) deg, amounting to a total area of ∼1 deg^2. The depth achieved (3 arcsec diameter aperture, 5σ detection) is fainter than 22 mag for filters bluewards of 7500 Å

[1] http://www.j-pas.org/

[2] http://svo2.cab.inta-csic.es/theory/fps/index.php?mode=browse&gname=OAJ&gname2=JPAS

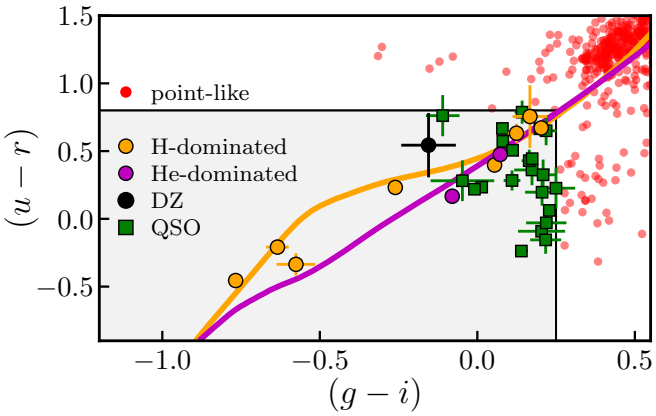

Fig. 1. $(u-r)$ vs. $(g-i)$ color–color diagram in miniJPAS for point-like sources with $r < 21.5$ mag (red dots). The gray area defines the bluest point-like sources with $(u-r) < 0.80$ mag and $(g-i) < 0.25$ mag. The 33 sources in this area are classified from the SDSS spectrum as 11 white dwarfs (eight with a H-dominated atmosphere, orange dots; two with a He-dominated atmosphere, purple dots; and one metal-polluted DZ, black dot) and 22 QSOs (green squares). The expected colors from theoretical cooling tracks for H-dominated and He-dominated atmospheres with $\log g = 8$ (Sect. 3) are shown with the orange and purple lines, respectively.

and ∼22 mag for longer wavelengths. The images and catalogs are publicly available on the J-PAS website[3].

We used the photometric data obtained with `SExtractor` (Bertin & Arnouts 1996) in the so-called dual mode. The r filter was used as the detection band and, for the rest of the filters, the aperture defined in the reference r-band was used to extract the flux. The observed fluxes in a 3 arcsec diameter aperture and their errors were stored in the vector $\boldsymbol{f} = \{f_j\}$ and $\sigma_f = \{\sigma_j\}$, where the index j runs the miniJPAS passbands, respectively. The error vector includes the uncertainties from photon counting and the sky background. Further details on the miniJPAS observations, data reduction, and photometric calibration can be found in Bonoli et al. (2021).

2.2. Aperture correction of the 3 arcsec photometry

The miniJPAS magnitudes measured in a 3 arcsec aperture are not the total magnitudes of the sources and an aperture correction is needed. The aperture correction was defined as

$$C^{\rm aper} = C_6^{\rm tot} + C_3^6. \quad (1)$$

The first term is the correction from 6 arcsec magnitudes to total magnitudes (i.e., the total flux of the star), which depends on the pointing and the filter. The second term corrects 3 arcsec photometry to 6 arcsec photometry and also depends on the position of the source in the CCD due to the variation of the point spread function along the FoV. The techniques and assumptions applied in the computation of these two aperture corrections are detailed in López-Sanjuan et al. (2022).

2.3. The sample of the bluest point-like sources

We aim to provide a forecast for the white dwarf science with the J-PAS 56 optical filters. Our working sample is composed of the bluest point-like sources (BPS) in the miniJPAS catalog, where mainly white dwarfs and extragalactic QSOs are expected. To define the BPS catalog, magnitudes from 3 arcsec photometry corrected by aperture effects were used.

The point-like sample was defined with apparent magnitude $r < 21.5$ mag to ensure there was a large enough signal-to-noise ratio (S/N) in medium-band photometry. This magnitude selection translates to a median S/N per passband larger than five in all the BPS. We also imposed a probability of being point-like of $p_{\rm point} > 0.5$. This probability was computed for each miniJPAS source with the Bayesian morphological classifier developed in López-Sanjuan et al. (2019) which is available in the miniJPAS database[4]. We obtained a total of 2684 sources with these criteria.

Then, a color selection was performed in the $(u-r)$ vs. $(g-i)$ color–color diagram (Fig. 1). We used these colors to ensure independent measurements and avoid correlated uncertainties. Several structures are apparent in this color-color plot. White dwarfs occupy the bluest corner in the plot, as illustrated with the H-dominated and He-dominated theoretical cooling tracks (see Sect. 3, for details about the assumed models). A sparsely populated sequence, corresponding to A-type and blue horizontal branch stars, is at $(g-i) \lesssim 0.3$ mag and $(u-r) \sim 1.2$ mag. The common F-type stars produce the overdensity at $(g-i) \sim 0.4$ mag and $(u-r) \sim 1.3$ mag. Finally, the QSO population is responsible for the data excess visible at $(g-i) \sim 0.3$ and $(u-r) \sim 0.3$ mag.

We defined the bluest sources in miniJPAS with $(u-r) < 0.80$ mag and $(g-i) < 0.25$ mag. These color selections ensure a complete sample for white dwarfs at $T_{\rm eff} \gtrsim 7000$ K, as is expected from the theoretical cooling tracks described in Sect. 3, and they minimize contamination from main sequence stars. The selection provided a total of 33 sources in the surveyed area of one square degree, defining the BPS sample.

The next step was to gather all the available information about the BPS in the literature. We searched for information in the Montreal white dwarf database[5] (Dufour et al. 2017) and Simbad[6] (Wenger et al. 2000). We also collected SDSS spectroscopy, *Gaia* DR3 astrometry (Gaia Collaboration 2021a), and *Gaia* DR3 BP/RP spectra (De Angeli et al. 2022). We found that all the BPS have a SDSS spectrum, providing a spectral classification of the sources.

The BPS sample was split into 11 white dwarfs (Tables 1–4) and 22 QSOs (Table 5). The physical properties of the white dwarfs are studied in Sect. 4, and the capabilities of miniJPAS photometry to disentangle between white dwarfs and QSOs are analyzed in Sect. 5.

3. Bayesian estimation of white dwarf atmospheric parameters and composition

The Bayesian methodology used to analyze the miniJPAS data was developed in López-Sanjuan et al. (2022) to study the white dwarf population in the Javalambre Photometric Local Universe Survey (J-PLUS, Cenarro et al. 2019), comprising 12 optical filters. We adapted the method to deal with the 56 medium bands in miniJPAS and we included the g and i broadbands in the analysis. The $u_{\rm J}$ and r broadbands were not used because they had been discarded from the final J-PAS observing strategy, which will only include g and i. In the following, we provide

[3] http://www.j-pas.org/datareleases/minijpas_public_data_release_pdr201912

[4] Variable `total_prob_star` stored in the table `minijpas.StarGalClass`

[5] http://www.montrealwhitedwarfdatabase.org

[6] http://simbad.u-strasbg.fr/simbad

Table 1. White dwarfs in the miniJPAS bluest point-like sample.

Tile–Number	SDSS name	RA [deg]	Dec [deg]	r [mag]	$(g-i)$ [mag]	$(u-r)$ [mag]
2241−1747	J141642.64+521543.4	214.1778	52.2620	19.32 ± 0.01	−0.08 ± 0.01	0.17 ± 0.02
2241−19527	J141800.78+522439.6	214.5030	52.4108	19.61 ± 0.01	−0.26 ± 0.02	0.23 ± 0.03
2243−2625	J141724.11+525227.5	214.3501	52.8745	19.30 ± 0.01	0.05 ± 0.01	0.40 ± 0.04
2243−4859	J141900.88+524354.6	214.7533	52.7319	21.48 ± 0.04	−0.15 ± 0.09	0.54 ± 0.24
2243−5175	J141951.40+523716.3	214.9642	52.6212	21.12 ± 0.03	−0.58 ± 0.06	−0.34 ± 0.08
2406−5601	J142125.69+530454.3	215.3567	53.0818	19.00 ± 0.01	0.20 ± 0.01	0.67 ± 0.03
2406−9645	J142032.63+531624.3	215.1359	53.2736	19.33 ± 0.01	0.07 ± 0.01	0.47 ± 0.03
2406−16326	J142249.53+530530.0	215.7065	53.0915	21.12 ± 0.03	0.17 ± 0.06	0.76 ± 0.23
2470−3588	J141348.35+520925.4	213.4513	52.1572	19.84 ± 0.01	−0.77 ± 0.02	−0.46 ± 0.02
2470−13619	J141613.45+521137.0	214.0558	52.1936	20.46 ± 0.01	0.12 ± 0.03	0.63 ± 0.07
2470−15262	J141611.12+520758.3	214.0462	52.1328	20.55 ± 0.02	−0.63 ± 0.04	−0.21 ± 0.04

Table 2. White dwarfs in the miniJPAS bluest point-like sample: *Gaia* DR3 information.

Tile–Number	Source ID	G [mag]	$G_{BP}-G_{RP}$ [mag]	ϖ_{DR3} [mas]	BP/RP spectra (a)	GF21 (b)
2241−1747	1607896637338835712	19.776 ± 0.004	−0.160 ± 0.049	4.36 ± 0.34	No	No
2241−19527	1607904501422166144	19.663 ± 0.003	−0.217 ± 0.065	4.95 ± 0.24	Yes	Yes
2243−2625	1608021500627073408	19.358 ± 0.002	0.026 ± 0.040	5.37 ± 0.19	Yes	Yes
2243−4859	···	···	···	···	No	No
2243−5175	1607958068254260480	20.99 ± 0.015	−0.69 ± 0.326	−2.6 ± 1.5	No	No
2406−5601	1607993944116951168	19.077 ± 0.002	0.211 ± 0.033	7.35 ± 0.15	Yes	Yes
2406−9645	1608048159488726272	19.402 ± 0.002	0.117 ± 0.056	6.31 ± 0.19	Yes	Yes
2406−16326	1608366506759904896	21.237 ± 0.025	−0.24 ± 0.42	···	No	No
2470−3588	1608068088137367168	19.731 ± 0.003	−0.760 ± 0.073	1.49 ± 0.24	No	Yes
2470−13619	1607884473991469312	20.523 ± 0.006	−0.07 ± 0.13	1.99 ± 0.55	No	Yes
2470−15262	1607884023018783232	20.491 ± 0.006	−0.39 ± 0.13	0.37 ± 0.53	No	No

Notes. (a) Low-resolution spectra from *Gaia* DR3 available (De Angeli et al. 2022); (b) included in the Gentile Fusillo et al. (2021) catalog based on *Gaia* DR3 with white dwarf probability $P_{WD} > 0.75$.

Table 3. White dwarfs in the miniJPAS bluest point-like sample: Atmospheric parameters from SDSS spectroscopy.

Tile–Number	SDSS Plate-MJD-Fiber	Type	Composition	$T_{\rm eff}^{\rm spec}$ [K]	$\log g^{\rm spec}$ [dex]	Reference
2241−1747	7028-56449-0220	DA	He	5240 ± 130	7.6 ± 0.3	2
2241−19527	7028-56449-0185	DA	H	11 010 ± 100	8.70 ± 0.06	2
2243−2625	7028-56449-0199	DA	H	7 880 ± 60	7.85 ± 0.11	2
2243−4859	7030-56448-0227	DZ	He	···	···	···
2243−5175	7028-56449-0102	DA	H	19 300 ± 700	8.17 ± 0.11	1
2406−5601	7028-56449-0930	DA	H	7380 ± 50	7.78 ± 0.11	2
2406−9645	6717-56397-0721	DC	He	···	···	···
2406−16326	7031-56449-0616	DA	H	7400 ± 300	8 ± 1	1
2470−3588	7030-56448-0453	DA	H	22 800 ± 400	7.89 ± 0.06	2
2470−13619	7030-56448-0380	DA	H	8520 ± 120	7.7 ± 0.2	2
2470−15262	7029-56455-0253	DA	H	17 600 ± 500	7.76 ± 0.09	1

References. (1) Kepler et al. (2016); (2) Kepler et al. (2019).

a summary of the fitting process, which is fully detailed in López-Sanjuan et al. (2022).

We estimated the normalized probability density function (PDF) for each white dwarf in the sample,

$$\mathrm{PDF}\,(t,\theta|\boldsymbol{f},\boldsymbol{\sigma_f}) \propto \mathcal{L}\,(\boldsymbol{f}|t,\theta,\sigma_f) \times P\,(\varpi), \quad (2)$$

where $t = \{\mathrm{H},\mathrm{He}\}$ are the explored H- and He-dominated atmosphere compositions, $\theta = \{T_{\rm eff}, \log g, \varpi\}$ are the parameters in the fitting (effective temperature, surface gravity, and parallax), $\mathcal{L}$ is the likelihood of the data for a given set of parameters and atmospheric composition, and P is the prior probability imposed on the parallax.

Table 4. White dwarfs in the miniJPAS bluest point-like sample: Fitting results from miniJPAS photometry.

Tile–Number	$p_{\rm H}$	$T_{\rm eff}$ [K]	log g [dex]	ϖ [mas]	$\chi^2_{\rm WD}$
2241−1747	0.00	8 510 ± 120	7.69 ± 0.14	4.4 ± 0.3	20.0 [(a)]
2241−19527	1.00	11 250 ± 240	8.66 ± 0.06	4.99 ± 0.24	33.7 [(a)]
2243−2625	1.00	7850 ± 100	7.91 ± 0.07	5.40 ± 0.19	18.4 [(a)]
2243−4859	0.88	8700 ± 400	7.0 ± 0.7	1.16 ± 0.23	81.3 [(a)]
2243−4859	0.01	8800 ± 400	8.3 ± 0.6	2.2 ± 1.0	53.2 [(b)]
2243−5175	1.00	19 900 ± 1100	7.8 ± 0.5	0.9 ± 0.3	52.9 [(a)]
2406−5601	1.00	7160 ± 80	7.95 ± 0.04	7.35 ± 0.15	13.2 [(a)]
2406−9645	0.00	7510 ± 90	7.99 ± 0.06	6.30 ± 0.19	36.7 [(a)]
2406−16326	0.99	7150 ± 180	8.8 ± 0.7	5.2 ± 3.4	48.3 [(a)]
2470−3588	1.00	22 400 ± 900	7.87 ± 0.22	1.45 ± 0.20	47.8 [(a)]
2470−13619	1.00	8140 ± 180	7.1 ± 0.4	1.99 ± 0.25	44.9 [(a)]
2470−15262	1.00	18 000 ± 800	7.6 ± 0.3	1.02 ± 0.21	52.8 [(a)]

Notes. [(a)]All the miniJPAS passbands were used in the fitting. [(b)]Passbands *J*0390 and *J*0400 were removed in the analysis (Sect. 4.1.3).

Table 5. Quasi-stellar objects in the miniJPAS bluest point-like sample.

Tile–Number	RA [deg]	Dec [deg]	r [mag]	$(g-i)$ [mag]	$(u-r)$ [mag]	$\varpi_{\rm DR3}$ [mas]	$z_{\rm spec}$	$\chi^2_{\rm WD}$
2241−3755	213.9637	52.4613	19.73 ± 0.01	0.20 ± 0.02	0.66 ± 0.04	−0.20 ± 0.28	2.581	314.0
2241−7683	214.3127	52.3869	21.24 ± 0.03	0.20 ± 0.07	−0.09 ± 0.08	···	1.260	131.4
2241−9344	214.4118	52.3925	21.26 ± 0.03	0.17 ± 0.06	0.36 ± 0.11	···	2.159	472.2
2241−14404	214.3972	52.6476	20.24 ± 0.01	0.14 ± 0.02	−0.24 ± 0.03	0.17 ± 0.44	1.961	520.8
2241−20770	214.5971	52.6679	21.28 ± 0.03	0.21 ± 0.05	0.20 ± 0.10	···	1.766	284.1
2243−12132	215.0233	53.0102	19.81 ± 0.01	0.23 ± 0.02	0.06 ± 0.04	−0.18 ± 0.28	1.647	431.4
2243−12352	214.9700	53.0345	20.47 ± 0.02	0.11 ± 0.03	0.28 ± 0.07	1.76 ± 0.74	1.902	265.3
2243−12363	214.9946	53.0194	20.83 ± 0.02	0.21 ± 0.04	0.32 ± 0.11	−1.03 ± 0.72	1.728	200.7
2406−853	215.2185	52.9396	18.14 ± 0.01	0.01 ± 0.01	0.23 ± 0.01	0.09 ± 0.08	0.676	430.4
2406−1224	215.3250	52.8961	20.39 ± 0.01	0.16 ± 0.02	0.43 ± 0.08	0.43 ± 0.37	2.305	577.3
2406−4342	215.0437	53.2066	20.09 ± 0.01	0.14 ± 0.02	0.79 ± 0.09	−0.68 ± 0.46	2.590	263.8
2406−5133	215.3823	53.0450	21.26 ± 0.03	−0.05 ± 0.10	0.28 ± 0.15	···	0.957	145.0
2406−8977	215.3053	53.2052	21.21 ± 0.03	0.22 ± 0.05	−0.16 ± 0.10	···	1.953	204.5
2406−11608	215.7752	53.2581	18.44 ± 0.01	0.08 ± 0.01	0.67 ± 0.02	−0.15 ± 0.13	2.462	481.1
2406−14008	215.6897	53.2010	21.34 ± 0.03	0.25 ± 0.06	0.26 ± 0.15	···	1.671	99.6
2406−14869	215.4022	53.3373	21.48 ± 0.04	0.22 ± 0.06	−0.03 ± 0.14	···	2.019	160.9
2470−2363	213.7993	51.8822	19.60 ± 0.01	0.08 ± 0.01	0.57 ± 0.03	−0.01 ± 0.22	2.306	350.4
2470−4230	213.4213	52.2056	18.96 ± 0.01	0.17 ± 0.01	0.44 ± 0.02	−0.05 ± 0.21	1.213	127.7
2470−4455	213.4495	52.2014	21.16 ± 0.03	−0.11 ± 0.05	0.76 ± 0.15	···	2.351	159.8
2470−7732	213.8912	52.0994	18.15 ± 0.01	−0.01 ± 0.01	0.22 ± 0.01	−0.03 ± 0.10	0.987	198.3
2470−9064	213.4318	52.3207	20.49 ± 0.02	0.22 ± 0.03	0.65 ± 0.11	−0.94 ± 0.62	1.327	258.8
2470−13393	213.6948	52.4233	19.47 ± 0.01	0.11 ± 0.01	0.51 ± 0.03	−0.48 ± 0.26	1.583	313.7

The likelihood was defined as

$$\mathcal{L}(\boldsymbol{f}|t,\theta,\sigma_f) = \prod_{j=1}^{58} P_{\rm G}\left(f_j|f_{t,j}^{\rm mod},\sigma_j\right), \quad (3)$$

where the index j runs over the 56 medium bands and the gi broadbands in miniJPAS, the function $P_{\rm G}$ defines a Gaussian distribution with median μ and dispersion σ, and the model flux was

$$f_{t,j}^{\rm mod}(t,\theta) = \left(\frac{\varpi}{100}\right)^2 F_{t,k}\left(T_{\rm eff},\log g\right) 10^{0.4\,k_j\,E(B-V)}\, 10^{0.4\,C_j^{\rm aper}}, \quad (4)$$

where k_j is the extinction coefficient of the filter, $E(B-V)$ is the color excess of the source, $C_j^{\rm aper}$ is the aperture correction needed to translate the observed 3 arcsec fluxes to total fluxes (Sect. 2.2), and $F_{t,k}$ is the theoretical absolute flux emitted by a white dwarf at a 10 pc distance. The uncertainty in the photometric calibration ($\sigma_{\rm cal} = 0.04$ mag) was included in the error vector.

The color excess was estimated by using the 3D reddening map from Green et al. (2018)[7] at distance $d = \varpi^{-1}$. We note that this extinction correction was used in the photometric calibration of miniJPAS, so we also used it for consistency.

Pure-H models were assumed to describe H-dominated atmospheres (t = H, Tremblay et al. 2011, 2013). Mixed models with H/He = 10^{-5} at $T_{\rm eff} > 6500$ K and pure-He models at

[7] We used the `Bayesta17` version of the map, available at `http://argonaut.skymaps.info`

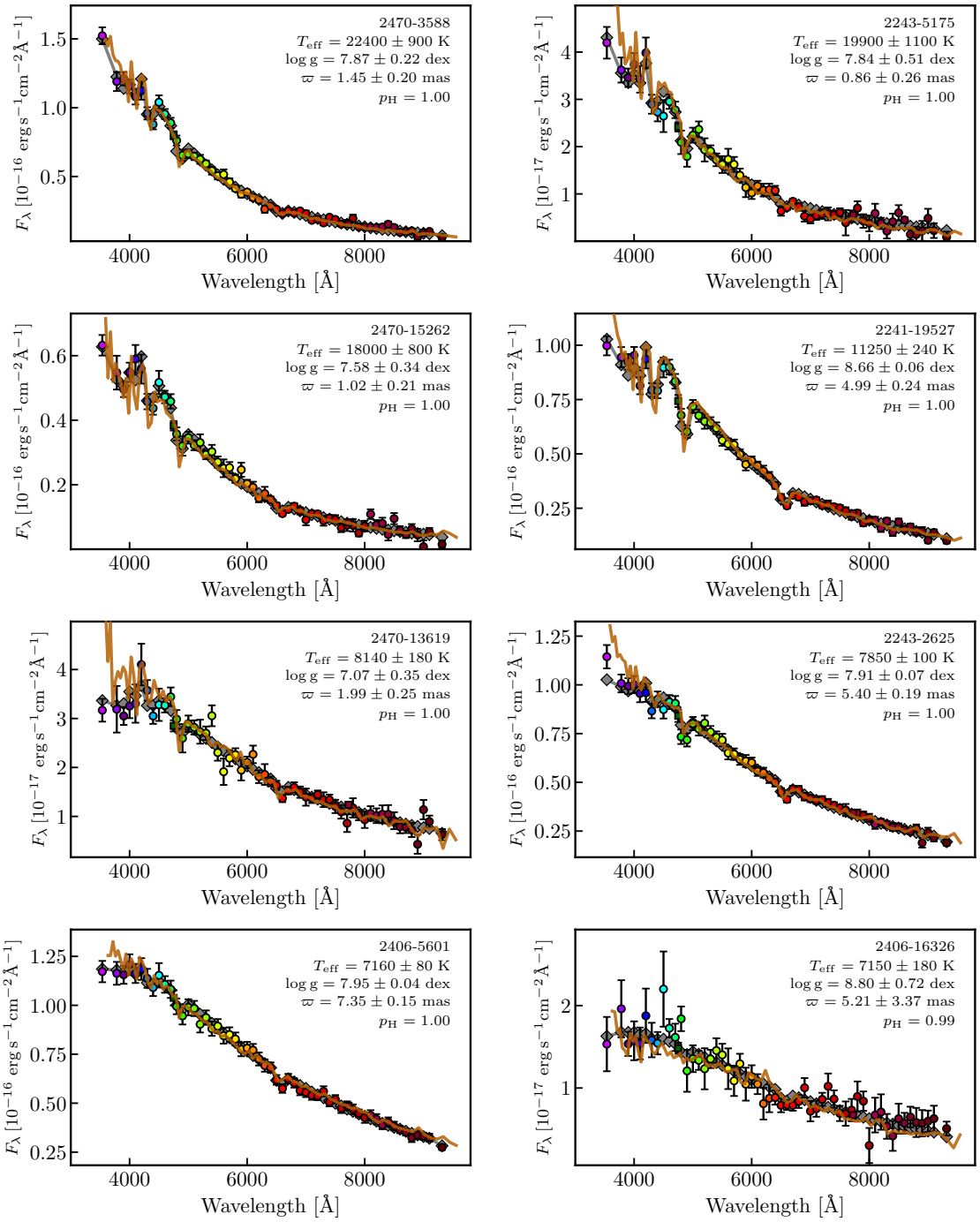

Fig. 2. Photo-spectra of the miniJPAS sources classified as H-dominated DAs in descending effective temperature from the top-left to bottom-right corner. Colored circles represent the 56 medium bands, and squares indicate the *g* and *i* broadbands. The presented fluxes were estimated from the 3 arcsec diameter aperture photometry corrected for aperture effects (Sect. 2.2), and no correction for interstellar reddening was applied. The gray diamonds show the theoretical flux from the best-fitting model to the data. The parameters of the fitting are labeled in the panels. The solid brown line depicts the SDSS spectra of the sources with a downgraded resolution of $R \sim 90$ for a better comparison. The flux of the SDSS spectra were scaled to match the miniJPAS *r*-band photometry. The flux scale of the SDSS spectra for the sources 2243−2625, 2406−5601, and 2406−16326 has an additional factor $(\lambda/\lambda_0)^a$ applied, with $\lambda_0 = 6254$ Å and $a = 1.1, 0.3$, and -0.4, respectively.

$T_{\rm eff} < 6500$ K were used to define He-dominated atmospheres (t = He, Cukanovaite et al. 2018, 2019). The mass-radius relation of Fontaine et al. (2001) for thin (He atmospheres) and thick (H atmospheres) hydrogen layers were used in the modeling. The justification of these choices and further details about the assumed models can be found in Bergeron et al. (2019), Gentile Fusillo et al. (2020, 2021), and McCleery et al. (2020).

The prior probability in the parallax was

$$P(\varpi) = P_{\rm G}(\varpi|\varpi_{\rm DR3}, \sigma_\varpi), \quad (5)$$

where $\varpi_{\rm DR3}$ and σ_ϖ are the parallax and its error from *Gaia* DR3 (Gaia Collaboration 2021a; Lindegren et al. 2021b). The published values of the parallax were corrected using the prescription in Lindegren et al. (2021a). In all cases, only positive

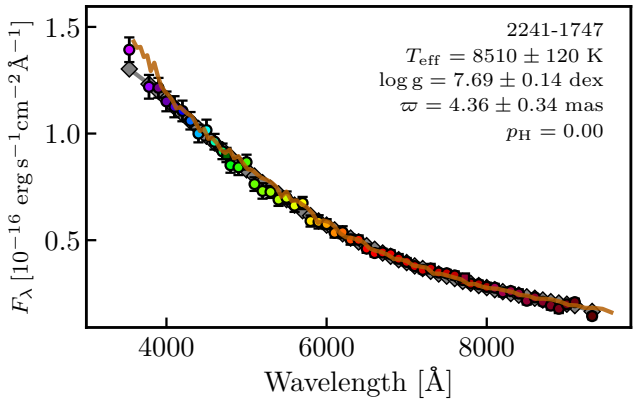

Fig. 3. Photo-spectrum of the miniJPAS source 2241–1747 (He-rich DA). Symbols are the same as in Fig. 2.

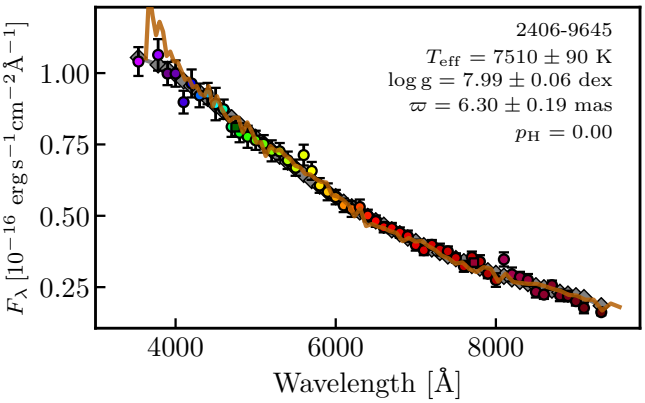

Fig. 4. Photo-spectrum of the miniJPAS source 2406–9645 (DC). Symbols are the same as in Fig. 2. The flux scale of the SDSS spectrum has an additional factor $(\lambda/\lambda_0)^{0.3}$ applied, with λ_0 = 6254 Å.

values of the parallax ($\varpi > 0$) were allowed. We note that the parallax posterior for those sources with a precise parallax measurement from *Gaia* DR3 resembles the high-quality input prior; whereas, for those sources with a low S/N parallax measurement or without entry in the *Gaia* catalog, the parallax posterior is only constrained by the miniJPAS photometry and exhibits larger uncertainties (Sect. 4.2).

Finally, the probability of having a H-dominated atmosphere was

$$p_{\rm H} = \int {\rm PDF}\,({\rm H}, \theta)\,{\rm d}\theta. \quad (6)$$

The reported values of each parameter in Table 4 were estimated by marginalizing over the other parameters at the dominant atmospheric composition defined by $p_{\rm H}$ and by performing a Gaussian fit to the obtained distribution. The parameter and its uncertainty are the median and the dispersion of the best-fitting Gaussian.

4. Analysis of the white dwarf population in miniJPAS

This section is devoted to the analysis of the white dwarf population in the BPS sample. We provide the relevant individual results for the 11 white dwarfs in Sect. 4.1. The performance in the estimation of the effective temperature and the surface gravity is presented in Sect. 4.2. The capabilities of the J-PAS filter system to derive the white dwarf atmospheric composition are discussed in Sect. 4.3.

4.1. Notes on individual objects

In this section, we present the relevant results for the nine DAs (Sect. 4.1.1), the DC (Sect. 4.1.2), and the DZ (Sect. 4.1.3) in the BPS sample. All the sources have a SDSS spectrum, but in several cases a mismatch between the spectrum and the miniJPAS photometry was evident. Such discrepancies have also been reported by Hollands et al. (2017). We found that both data sets can be reconciled by simply multiplying the SDSS spectrum by a factor $(\lambda/\lambda_0)^a$, with λ_0 = 6254 Å and a different index a for each individual source.

4.1.1. DA spectral type

There are eight H-dominated DAs and one He-rich DA in the analyzed sample. The H-dominated sources are presented in Fig. 2 and ordered by decreasing effective temperature. We find that the miniJPAS photometry shows Hα, Hβ, Hγ, and Hδ in most of the cases. The intensity of the Balmer lines is also recovered by the miniJPAS photo-spectra well. We obtained $p_{\rm H} \geq 0.99$ for all the H-dominated DAs. The effective temperature and surface gravity from miniJPAS photometry are compatible with the spectroscopic values at a 2σ level in all of the cases (Sect. 4.2).

The source 2241−1747 is spectroscopically classified as a He-rich DA by Kepler et al. (2016), but it was classified as DC in previous studies because of its weak Balmer lines (Eisenstein et al. 2006; Kleinman et al. 2013). The analysis of the spectrum with pure-H models implies $T_{\rm eff} \sim 5200$ K, but the continuum suggests a hotter system. Both results can be reconciled with a He-dominated atmosphere (see Rolland et al. 2018; Kilic et al. 2020). The miniJPAS data provide a featureless photo-spectrum (Fig. 3) with $p_{\rm H} = 0$ and a shape compatible with the SDSS spectrum of the source. As expected, the photometric effective temperature is $T_{\rm eff}$ = 8510 ± 120 K, thus it is hotter by ∼3000 K than the reported spectroscopic value when a pure-H atmosphere is assumed.

4.1.2. DC spectral type

The source 2406−9645 is the only object in the sample classified as DC (Fig. 4). The miniJPAS photometry is compatible with a featureless continuum, providing $p_{\rm H} = 0$. We estimated $T_{\rm eff}$ = 7510 ± 90 K and log g = 7.99 ± 0.06 dex.

4.1.3. DZ spectral type

The source 2243−4859 is classified as DZ (calcium white dwarf; Fig. 5), and the Ca II H+K absorption feature is present at 3950 Å in the SDSS spectrum. The miniJPAS photometry presents clear absorption in the passbands $J0390$ and $J0400$. The parameters obtained with all the photometric data provides $p_{\rm H}$ = 0.88 and a low surface gravity of log g = 7.0±0.7 dex. We repeated the analysis without the $J0390$ and $J0400$ passbands. The solutions in this case are different, with $p_{\rm H}$ = 0.01 and log g = 8.3 ± 0.6 dex. In both cases, the effective temperature is similar, $T_{\rm eff} \sim 8800$ K. We note that this object has no parallax information from *Gaia* DR3. We compared the expected flux in the $J0390$ passband from the latter fitting process with the miniJPAS measurement, obtaining an equivalent width (EW) of EW$_{J0390}$ = 78 ± 12 Å, or

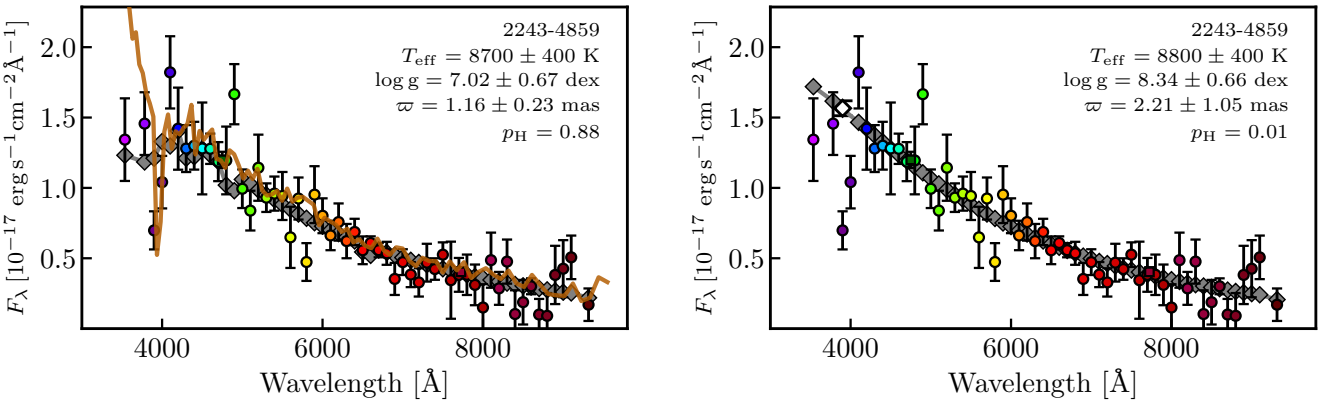

Fig. 5. Photo-spectrum of the miniJPAS source 2243-4859 (DZ). Symbols are the same as in Fig. 2. *Left panel*: all of the miniJPAS passbands were used in the fitting process. *Right panel*: filters *J*0390 and *J*0400 were not included in the fitting. The expected flux in the *J*0390 passband from the modeling is marked by a white diamond.

a 6σ detection of the calcium absorption. The J-PAS capabilities to detect metal-polluted white dwarfs are discussed in Sect. 4.3.

4.2. Temperature and surface gravity

In this section, we compare the $T_{\rm eff}$ and $\log g$ values obtained from miniJPAS photometry against those obtained from SDSS spectroscopy by Kepler et al. (2016, 2019), as summarized in Table 3. The DAs spectra were fitted with pure-H models (Koester 2010), including the Stark-line broadening from Tremblay & Bergeron (2009) and the 3D corrections from Tremblay et al. (2013) at $T_{\rm eff} \leq 14\,000$ K. We restricted the comparison to the eight H-dominated white dwarfs in the sample (Sect. 4.1.1) for which the spectroscopic method based on pure-H theoretical models is reliable.

We found a tight one-to-one agreement in $T_{\rm eff}$, as illustrated in Fig. 6. The relative difference between both measurements is 1%, with a dispersion of only 3%. All the miniJPAS measurements are compatible with the spectroscopic values at a 2σ level. The typical relative error in the effective temperature from miniJPAS data is 2%, which is close to the 1% estimated from spectroscopy. Additionally, the typical relative error for the general white dwarf population is 10% from *Gaia* DR3 photometry (Gentile Fusillo et al. 2021) and 5% from J-PLUS photometry (López-Sanjuan et al. 2022).

As reported in Sect. 4.1, some SDSS spectra present a shape discrepancy with the miniJPAS photometry. The excellent agreement between the effective temperature from the SDSS spectrum, which is based on the absorption features and is thus insensitive to flux normalization, and from miniJPAS photometry, mainly based on the continuum shape, points to a problematic flux calibration of the discrepant SDSS spectra.

The surface gravity values obtained with both photo-spectra and spectroscopic data are compared in Fig. 7. We found agreement between photometric and spectroscopic measurements. However, a precise estimation of $\log g$ from miniJPAS photometry demands a precise parallax measurement from *Gaia*. The surface gravity information is mainly encoded in the widths of the lines, which are not accessible with the low-resolution miniJPAS photo-spectrum. The assumption of a mass-radius relation in the theoretical models couples the surface gravity and the parallax, so a precise parallax prior from *Gaia* astrometry permits one to derive the surface gravity when both the effective temperature and the atmospheric composition are well constrained.

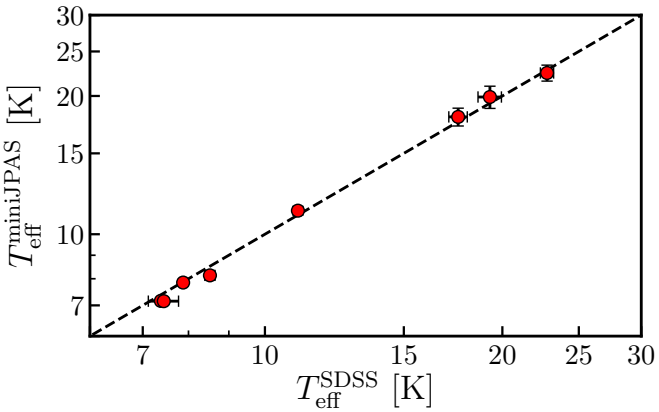

Fig. 6. Effective temperature derived from miniJPAS photometry, $T_{\rm eff}^{\rm miniJPAS}$, as a function of the effective temperature derived from the SDSS spectrum, $T_{\rm eff}^{\rm SDSS}$ (red dots with black error bars). The dashed line marks the one-to-one relation.

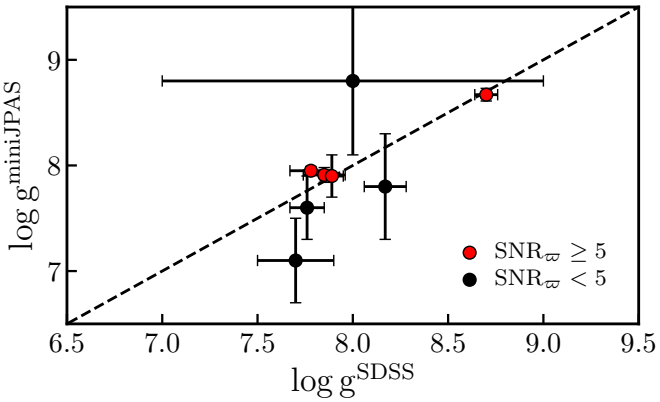

Fig. 7. Surface gravity derived from miniJPAS photometry, $\log g^{\rm miniJPAS}$, as a function of the surface gravity derived from the SDSS spectrum, $\log g^{\rm SDSS}$. Red dots mark sources with a S/N in $\varpi_{\rm DR3}$ larger than five, and black dots are sources with a S/N lower than five. The dashed line indicates the one-to-one relation.

We conclude that J-PAS is able to provide effective temperatures with ~2% precision. However, its spectral resolution is not large enough to retrieve a precise surface gravity without parallax information.

4.3. White dwarf atmospheric composition

The main advantage of low-resolution spectral information with respect to broadband photometry is its capability to disentangle the white dwarf main atmospheric composition and to identify the presence of polluting metals. The miniJPAS medium-band photometry permitted us to classify, with 99% confidence, the 11 white dwarfs in the sample correctly. The hydrogen Balmer lines are visible in miniJPAS photometry of H-dominated atmospheres with temperatures ranging from 7000 K to 22 000 K. The lack of He-dominated white dwarfs in miniJPAS at $T_{\rm eff}$ > 9000 K can be circumvented thanks to the results obtained with J-PLUS by López-Sanjuan et al. (2022). These authors analyzed 5926 white dwarfs using a 12 passbands filter system (*ugriz* and seven medium bands) to derive the evolution with effective temperature in the fraction of He-dominated white dwarfs. They also compared their photometric classification with the spectroscopic class for 1218 white dwarfs ranging from 5000 K to 30 000 K. They conclude that H- and He-dominated atmospheres can be correctly classified in J-PLUS at 9000 < $T_{\rm eff}$ < 17 000 K. The spectral resolution provided by the J-PLUS filter system is lower than the J-PAS resolution, and we can therefore assume that the J-PLUS capabilities will be achieved by J-PAS. The miniJPAS results permit the performance to be extended to the range 7000 < $T_{\rm eff}$ < 9000 K, where H- and He-dominated white dwarfs have been observed and properly classified. Moreover, the sensitivity of the J-PAS filter system to the presence of the Balmer series at $T_{\rm eff}$ > 17 000 K suggests that the high temperature limit in J-PLUS will also be improved. Our results point that the future J-PAS data would allow one to classify white dwarfs as H- and He-dominated at least from 7000 K to 22 000 K, which is the temperature range covered by the current sample. The J-PAS performance at even lower and higher effective temperatures will be tested in the near future when larger samples are available.

The presence of polluting metals in the white dwarf atmosphere can be identified thanks to the filters *J*0390 and *J*0400. These passbands are sensitive to the presence of Ca II H+K absorption, as illustrated for the source 2243−4859 in Fig. 5. We have estimated the EW in the *J*0390 filter as described in Sect. 4.1.3 for all the white dwarfs in the sample. The significance of the measurement, estimated as $\mathrm{EW}_{J0390}/\sigma_{\rm EW}$, is presented in Fig. 8. The non-DZ sources cluster around zero and are compatible with the absence of calcium absorption at the 2σ level. A Kolmogov-Smirnov test provides a 98% probability that their distribution is drawn for a normal distribution, as is expected if the measurements are compatible with zero within uncertainties. The only outlier is the DZ source, which presents a 6σ detection. Thus, the EW_{J0390} measurement can be used to select new metal-polluted white dwarfs. In addition to the calcium absorption, other prominent absorption features in cool white dwarfs, such as the Mg I *b* triplet and the Na I doublet at 5893 Å (e.g., Hollands et al. 2017), would also be present in the J-PAS data. The minimum EW detectable by the J-PAS filter system cannot be estimated with the limited miniJPAS sample. Fortunately, we can benefit again from the larger statistics from J-PLUS. We estimated the absorption EW for the 5 926 white dwarfs presented in López-Sanjuan et al. (2022) using the *J*0395 passband of FWHM = 100 Å in J-PLUS. The results will be presented in a forthcoming paper and demonstrate that J-PLUS medium-band photometry is sensitive to calcium absorption features with an EW larger than 15 Å. As previously mentioned, we can use the measured J-PLUS limit as a proxy for the J-PAS capabilities.

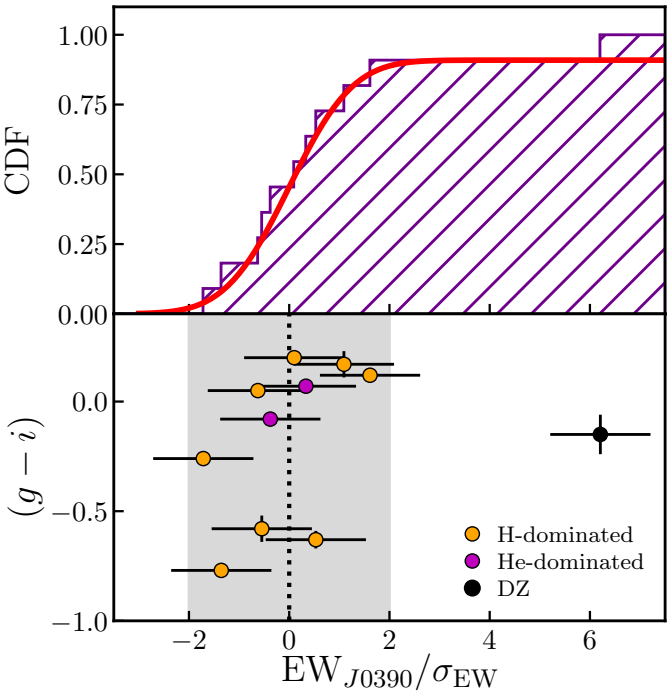

Fig. 8. Distribution in the significance of the EW_{J0390} measurements as a proxy for calcium absorption in white dwarfs. *Top panel*: cumulative distribution function (CDF) of the EW_{J0390} significance. The solid red line is the CDF of a normal distribution normalized to the non-DZ population. *Bottom panel*: color $(g-i)$ as a function of the EW_{J0390} significance. Symbols are the same as in Fig. 1. The dotted line marks zero and the gray area shows the $\pm2\sigma$ interval.

The small sample available in the miniJPAS area and the lower spectral resolution of J-PLUS do not permit one to anticipate the J-PAS capabilities in either the classification and estimation of H-to-He abundances on hybrid types (e.g., DABs and DBAs) or the measurement of metal abundances in polluted systems. In addition, the miniJPAS sample does not contain magnetic, carbon, or peculiar white dwarfs. The performance of the J-PAS filter system with these types will be evaluated in the future when larger samples are observed.

We conclude that the J-PAS photo-spectrum would allow one to study the evolution of He-dominated white dwarfs and the fraction of metal-polluted white dwarfs with an effective temperature using a well-controlled selection function at least down to $T_{\rm eff} \sim 7000$ K.

5. White dwarf selection based on miniJPAS photometry

We have analyzed the capabilities of multi-band photometry in the study of known white dwarfs. This will impact the analysis of the future white dwarf samples, such as those expected from *Gaia* data. In addition, we aim to test the performance of miniJPAS data to select new white dwarf candidates just based on optical photo-spectra. In this section, we analyze the BPS sample in this regard. For that, the model flux presented in Sect. 2.2 was simplified as follows:

$$f_{t,j}^{\rm mod}(t, T_{\rm eff}, \log g) = C_r\, F_{t,k}(T_{\rm eff}, \log g)\, 10^{0.4\, k_j\, E(B-V)}\, 10^{0.4\, C_j^{\rm aper}}, \quad (7)$$

where C_r is a constant to normalize the theoretical flux to the measured flux in the miniJPAS r band. That is, we assumed a unique scale for each $\{T_{\rm eff}, \log g\}$ pair to remove the parallax as a parameter in the fitting process. The prior in parallax was also neglected to provide a consistent analysis of Galactic and extragalactic sources, and only the likelihood of being a white dwarf was computed. The assumed color excess was computed at the distance implied by the C_r normalization.

We used this scheme to obtain the minimum χ^2 for each object as

$$\chi^2_{\rm WD} = -2 \times \log \mathcal{L}_{\rm max}, \quad (8)$$

where $\mathcal{L}_{\rm max}$ is the maximum likelihood obtained in the exploration of the parameters' space for both H- and He-dominated atmospheres. We present the results in Fig. 9, and show the corresponding $\chi^2_{\rm WD}$ in Tables 4 and 5. We found a clear separation between white dwarfs and QSOs in the BPS sample in terms of their $\chi^2_{\rm WD}$, with white dwarfs having lower values.

We have 58 photometric points and three effective parameters when the constraints from the *Gaia* DR3 parallax are weak (López-Sanjuan et al. 2022). Thus, the values should tend to $\chi^2_{\rm WD} \approx 55$. The white dwarfs tend to $\chi^2_{\rm WD} \approx 53$ at the faint end, as expected. There is also a trend toward lower $\chi^2_{\rm WD}$ at brighter magnitudes ($r \lesssim 19.5$ mag), reflecting an overestimation of the uncertainty in the photometric calibration, which was set to $\sigma_{\rm cal} = 0.04$ mag for all the passbands. The QSOs have larger values of $\chi^2_{\rm WD}$, reaching even $\chi^2_{\rm WD} = 500$. This is due to the presence of emission lines, which are unexpected for white dwarfs. The presence of the Lyman α line in the QSO spectrum at $z > 2$ provides the most prominent differences.

We conclude that white dwarfs in the BPS sample can be selected with high confidence by imposing $\chi^2_{\rm WD} \leq 80$. High-purity white dwarf samples will be defined with J-PAS, thus complementing the astrometric information from *Gaia* down to $G \sim 21$ and permitting the analysis beyond *Gaia* capabilities. As an example, of the 33 sources in the BPS sample, ten (30%) do not have parallax in the *Gaia* DR3 catalog and only two of them are white dwarfs (Fig. 9).

The calcium white dwarf 2243−4859 presents $\chi^2_{\rm WD} = 81$ if all the passbands are used in the fitting; this value decreases to $\chi^2_{\rm WD} = 53$ when $J0390$ and $J0400$ are removed from the analysis. This implies that these two filters are clearly discrepant with the expected white dwarf flux due to the presence of calcium absorption, and they provide a way to select metal-polluted white dwarfs using multi-filter photometry (Sect. 4.3). We checked that no QSO were located below the $\chi^2_{\rm WD} = 80$ limit when the $J0390$ and $J0400$ passbands were removed from the analysis.

Finally, we searched for white dwarf candidates in the *Gaia*-based catalog presented by Gentile Fusillo et al. (2021). Following the authors' suggestion, we only kept those sources with a white dwarf probability larger than 0.75. We found six sources, all with $r < 20.5$ mag (Fig. 9 and Table 2). Two of the four sources with $r > 20.5$ mag present S/N < 1 in the parallax and the other two have no parallax measurement. There is one bright source that is not included in the catalog, 2241−1747. This source was discarded by Gentile Fusillo et al. (2021) because of the presence of a fainter, close source that increases the number of parameters in the solved astrometric solution[8]. This exercise suggests that the number of high-confidence white dwarfs in the J-PAS area could be doubled with respect to *Gaia*-based catalogs.

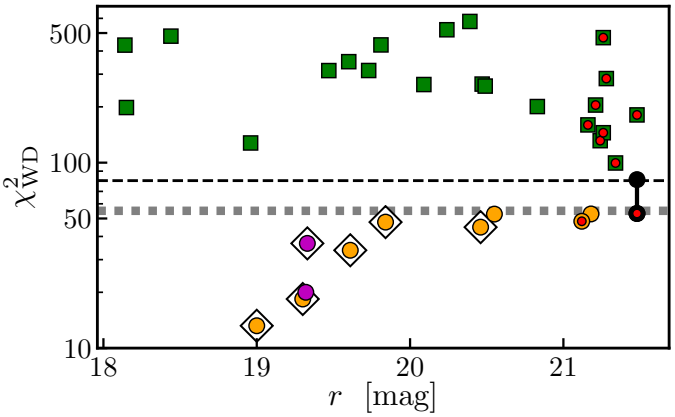

Fig. 9. Minimum $\chi^2_{\rm WD}$ as a function of the r-band magnitude for the BPS. Circles mark spectroscopic white dwarfs (H-dominated, orange; He-dominated, purple; and metal-polluted, black), and green squares show QSOs. The values obtained with and without the filters $J0390$ and $J0410$ for the calcium white dwarf 2243−4859 are connected by a black line. Those sources without *Gaia* DR3 parallax information are marked with a red dot. Those white dwarfs included in the Gentile Fusillo et al. (2021) catalog are marked with a white diamond. The black dashed line depicts the separation between white dwarfs and QSOs, $\chi^2_{\rm WD} = 80$. The dotted line shows the expected value for white dwarfs given the degrees of freedom in the analysis, $\chi^2_{\rm WD} = 55$.

A complete analysis of the BPS sample demands the addition of QSO models. This is beyond the scope of the present paper, and we demonstrated that the comparison between miniJPAS photometry and the white dwarf theoretical models is enough to discriminate the QSOs in the bluest sources at $r \leq 21.5$ mag thanks to the 56 medium bands in the J-PAS photometric system.

6. Discussion and conclusions

We have analyzed the physical properties of 11 white dwarfs in the miniJPAS data set, which provides a low-resolution photo-spectrum thanks to a unique filter system of 56 medium bands with FWHM $\approx$ 145 Å continuously covering the optical range from 3500 to 9300 Å.

We found that the effective temperature determination has a typical relative error of 2%, whereas the estimation of a precise surface gravity demands the parallax information from *Gaia*. Regarding the atmospheric composition, the J-PAS filter system would be able to correctly classify H- and He-dominated atmosphere white dwarfs, at least in the temperature range covered by the miniJPAS white dwarf sample, $7000 < T_{\rm eff} < 22\,000$ K. The presence of polluting metals can be revealed by the Ca II H+K absorption, as traced by the $J0390$ and $J0400$ passbands, for systems with an EW larger than 15 Å. Furthermore, the miniJPAS low-resolution information should be able to disentangle between white dwarfs with $T_{\rm eff} \gtrsim 7000$ K and extragalactic QSOs with similar broadband colors.

The J-PAS project, with thousands of square degrees observed in the northern sky, will provide a unique data set of several tens of thousands of white dwarfs down to $r \sim 21.5$ mag. This sample will be used to analyze the fraction of He-dominated white dwarfs with $T_{\rm eff}$, search for new metal-polluted systems, derive the white dwarf luminosity function, detect unusual objects, etc. In addition to the data-driven

[8] The values of the parameters ASTROMETRIC_PARAMS_SOLVED = 95, ASTROMETRIC_EXCESS_NOISE = 2.2, and ASTROMETRIC_EXCESS_NOISE_SIG = 8.3 do not fulfill the requirements imposed by Eq. (8) in Gentile Fusillo et al. (2021)

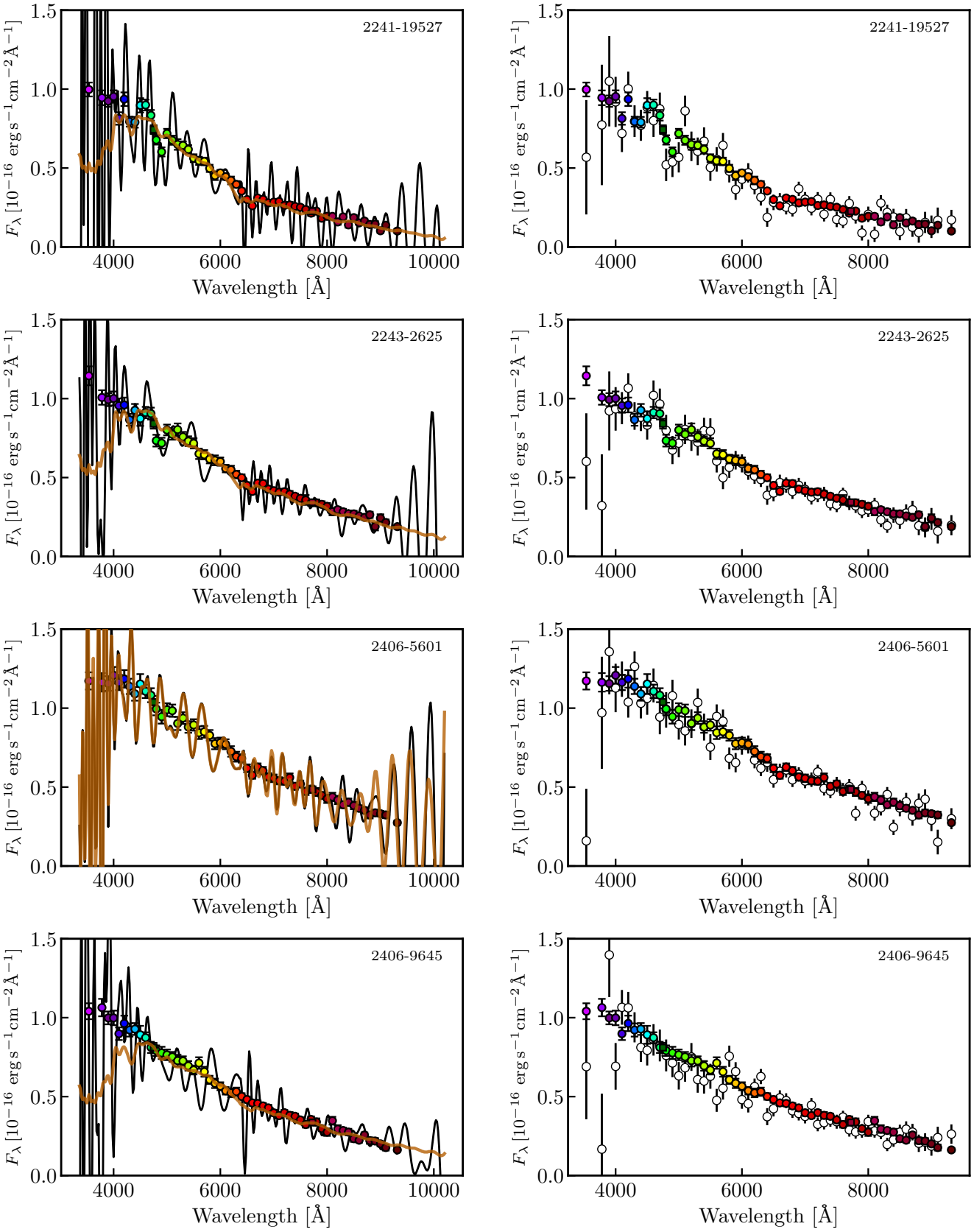

Fig. 10. Photo-spectra of the four miniJPAS sources with BP/RP spectra released in *Gaia* DR3. Colored symbols are the same as in Fig. 2. The solid black and brown lines in the *left panels* show the reconstructed spectra from the basis coefficients without and with truncation, respectively. The white dots in the *right panels* present the synthetic photometry computed from the BP/RP full reconstructed spectra and the J-PAS photometric system. No offset has been applied to the *Gaia* DR3 flux scale.

forecast for J-PAS, our results provide hints about the performance of the *Gaia* BP/RP spectra, complementing the results presented in Carrasco et al. (2014) and Gaia Collaboration (2022). The *Gaia* BP/RP spectra have a comparable resolution to miniJPAS data, $R = 30-90$, and therefore similar capabilities are expected at the same S/N level.

There are relevant synergies between *Gaia* and J-PAS that are worth noticing. On the one hand, *Gaia* provides a full sky data set. On the other hand, J-PAS is deeper and provides a high S/N photo-spectrum even at $G = 21$ mag. We envision three different regimes: (i) bright sources with enough S/N in *Gaia* BP/RP spectra. Two independent measurements of the white dwarf properties will be available, providing insight about systematic errors in both surveys and testing *Gaia* capabilities at the lower S/N. We also envisage (ii) faint sources with enough S/N in *Gaia* astrometry. The combination of J-PAS photo-spectra and *Gaia* parallaxes will permit one to define and study the white dwarf population down to $G \sim 21$ mag in detail. Lastly, we foresee (iii) white dwarf candidates beyond *Gaia* data, $G > 21$ mag. The J-PAS photo-spectrum can provide clean samples of white dwarfs for spectroscopic follow-up in a magnitude range dominated by QSOs and without the parallax information from *Gaia*. In this range, the main alternative will be the use of reduced proper motions for deep, multi-epoch surveys such as the Legacy Survey for Space and Time (LSST, Ivezic et al. 2019), which is capable of obtaining reliable white dwarf candidates down to $G \sim 23$ mag (Fantin et al. 2020).

As an illustrative example of case (iii), the 11 white dwarfs in the miniJPAS area are made up of the following: six sources (55%) included in the Gentile Fusillo et al. (2021) catalog based on *Gaia* DR3 with a white dwarf probability larger than 0.75; three sources (27%) with a low S/N or a low quality flag in *Gaia* and not included in the Gentile Fusillo et al. (2021) catalog; and two white dwarfs (18%) without a parallax entry on the *Gaia* DR3 catalog. Hence, there is potential to double the number of high-confidence white dwarf candidates in the future J-PAS area with respect to the *Gaia*-based catalogs. However, this will depend on the S/N achieved at the final *Gaia* data release.

Moreover, there are four white dwarfs in miniJPAS with published BP/RP spectra from *Gaia* DR3 (De Angeli et al. 2022). This permits one to evaluate case (ii) because of the typical magnitude of the sources, with $G > 19$ mag in all cases. The comparison between the miniJPAS photometry, the reconstructed spectra from the released basis coefficients in *Gaia* DR3, and the synthetic photometry computed using the J-PAS photometric system over the BP/RP spectra is presented in Fig. 10. Several lessons can already be learned from this limited sample. First, the photometric scales of miniJPAS and *Gaia* seem similar (see also Gaia Collaboration 2022). Second, the reconstructed spectra present well-known wiggles due to limitations in the reconstruction process (Montegriffo et al. 2022). The truncation of the basis used in the reconstruction following the prescriptions in De Angeli et al. (2022) does not improve the results, with similar recovered spectra for three of the sources (2241−19527, 2243−2625, and 2406−9645) and a discrepant shape with respect to the miniJPAS photometry at $\lambda \lesssim 4500$ Å. This is especially worrisome for the DC source 2406−9645. Truncation does not seem to work properly on source 2406−5601. This exercise already suggests that truncation should be avoided in the analysis of the *Gaia* DR3 white dwarf sample presented by Gaia Collaboration (2022). Third, the comparison with the J-PAS synthetic photometry computed from the BP/RP spectra is more satisfactory, especially at $\lambda > 4000$ Å (right panels in Fig. 10). There are hints of Hβ absorption in 2241−19527 and 2243−2625. The J-PAS photometric system has a spectral resolution comparable with the nominal BP/RP resolution (Montegriffo et al. 2022), and the spectra were therefore integrated over a more natural scale reducing the impact of the wiggles. Finally, the median S/N per passband in miniJPAS (S/N ≈ 20) is three times larger than in the synthetic photometry from BP/RP spectra (S/N ≈ 7).

To conclude, the J-PAS photo-spectra will complement the spectroscopic follow-up of the *Gaia*-selected white dwarf population planned with SDSS-V, WEAVE, and DESI in the northern sky. J-PAS will detect and characterize new white dwarfs beyond the *Gaia* limits, improving the selection function of the spectroscopic surveys and providing extra candidates for spectroscopic follow-up.

Acknowledgements. We dedicate this paper to the memory of our six IAC colleagues and friends who met with a fatal accident in Piedra de los Cochinos, Tenerife, in February 2007, with special thanks to Maurizio Panniello, whose teachings of `python` were so important for this paper. This paper has gone through internal review by the J-PAS collaboration, with relevant comments and suggestions from A. Bragaglia and A. Alvarez-Candal. We thank the anonymous referee for useful comments and suggestions. Based on observations made with the JST250 telescope and PathFinder camera for the miniJPAS project at the Observatorio Astrofísico de Javalambre (OAJ), in Teruel, owned, managed, and operated by the Centro de Estudios de Física del Cosmos de Aragón (CEFCA). We acknowledge the OAJ Data Processing and Archiving Unit (UPAD) for reducing and calibrating the OAJ data used in this work. Funding for OAJ, UPAD, and CEFCA has been provided by the Governments of Spain and Aragón through the Fondo de Inversiones de Teruel; the Aragonese Government through the Research Groups E96, E103, E16_17R, and E16_20R; the Spanish Ministry of Science, Innovation and Universities (MCIU/AEI/FEDER, UE) with grant PGC2018-097585-B-C21; the Spanish Ministry of Economy and Competitiveness (MINECO/FEDER, UE) under AYA2015-66211-C2-1-P, AYA2015-66211-C2-2, AYA2012-30789, and ICTS-2009-14; and European FEDER funding (FCDD10-4E-867, FCDD13-4E-2685). Funding for the J-PAS Project has been provided by the Governments of Spain and Aragón through the Fondo de Inversiones de Teruel, European FEDER funding and the Spanish Ministry of Science, Innovation and Universities, and by the Brazilian agencies FDNCT, FINEP, FAPESP, FAPERJ and by the National Observatory of Brazil. Additional funding was also provided by the Tartu Observatory and by the J-PAS Chinese Astronomical Consortium. P.-E. T. has received funding from the European Research Council under the European Union's Horizon 2020 research and innovation programmes n. 677706 (WD3D) and n. 101002408 (MOS100PC). A. E. and J. A. F. O. acknowledge the financial support from the Spanish Ministry of Science and Innovation and the European Union - NextGenerationEU through the Recovery and Resilience Facility project ICTS-MRR-2021-03-CEFCA. M. A. G. is funded by the Spanish Ministerio de Ciencia, Innovación y Universidades (MCIU) grant PGC2018-102184-B-I00, co-funded by FEDER funds. He also acknowledges support from the State Agency for Research of the Spanish MCIU through the "Center of Excellence Severo Ochoa" award to the Instituto de Astrofísica de Andalucía (SEV-2017-0709). J. V. acknowledges the technical members of the UPAD for their invaluable work: Juan Castillo, Tamara Civera, Javier Hernández, Ángel López, Alberto Moreno, and David Muniesa. F. M. J. E. acknowledges financial support from the Spanish MINECO/FEDER through the grant AYA2017-84089 and MDM-2017-0737 at Centro de Astrobiología (CSIC-INTA), Unidad de Excelencia María de Maeztu, and from the European Union's Horizon 2020 research and innovation programme under Grant Agreement no. 824064 through the ESCAPE – The European Science Cluster of Astronomy and Particle Physics ESFRI Research Infrastructures project. R. L. O. acknowledges financial support from the Brazilian institutions CNPq (PQ-312705/2020-4) and FAPESP (#2020/00457-4). R. A. D. acknowledges support from the Conselho Nacional de Desenvolvimento Científico e Tecnológico – CNPq through BP grant 308105/2018-4, and the Financiadora de Estudos e Projetos – FINEP grants REF. 1217/13 – 01.13.0279.00 and REF 0859/10 – 01.10.0663.00 and also FAPERJ PRONEX grant E-26/110.566/2010 for hardware funding support for the J-PAS project through the National Observatory of Brazil and Centro Brasileiro de Pesquisas Físicas. L. S. J. acknowledges the support of CNPq (304819/2017-4) and FAPESP (2019/10923-5). This work has made use of data from the European Space Agency (ESA) mission *Gaia* (`https://www.cosmos.esa.int/gaia`), processed by the *Gaia* Data Processing and Analysis Consortium (DPAC, `https://www.cosmos.esa.int/web/gaia/dpac/consortium`). Funding for the DPAC has been provided by national institutions, in particular the institutions participating in the *Gaia* Multilateral Agreement. This job has made use of the Python package `GaiaXPy`,

developed and maintained by members of the *Gaia* Data Processing and Analysis Consortium (DPAC), and in particular, Coordination Unit 5 (CU5), and the Data Processing Centre located at the Institute of Astronomy, Cambridge, UK (DPCI). Funding for the Sloan Digital Sky Survey IV has been provided by the Alfred P. Sloan Foundation, the U.S. Department of Energy Office of Science, and the Participating Institutions. SDSS-IV acknowledges support and resources from the Center for High Performance Computing at the University of Utah. The SDSS website is `www.sdss.org`. SDSS-IV is managed by the Astrophysical Research Consortium for the Participating Institutions of the SDSS Collaboration including the Brazilian Participation Group, the Carnegie Institution for Science, Carnegie Mellon University, Center for Astrophysics | Harvard and Smithsonian, the Chilean Participation Group, the French Participation Group, Instituto de Astrofísica de Canarias, The Johns Hopkins University, Kavli Institute for the Physics and Mathematics of the Universe (IPMU)/University of Tokyo, the Korean Participation Group, Lawrence Berkeley National Laboratory, Leibniz Institut für Astrophysik Potsdam (AIP), Max-Planck-Institut für Astronomie (MPIA Heidelberg), Max-Planck-Institut für Astrophysik (MPA Garching), Max-Planck-Institut für Extraterrestrische Physik (MPE), National Astronomical Observatories of China, New Mexico State University, New York University, University of Notre Dame, Observatário Nacional/MCTI, The Ohio State University, Pennsylvania State University, Shanghai Astronomical Observatory, United Kingdom Participation Group, Universidad Nacional Autónoma de México, University of Arizona, University of Colorado Boulder, University of Oxford, University of Portsmouth, University of Utah, University of Virginia, University of Washington, University of Wisconsin, Vanderbilt University, and Yale University. This research has made use of the SIMBAD database, operated at CDS, Strasbourg, France. This research made use of `Astropy`, a community-developed core `Python` package for Astronomy (Astropy Collaboration 2013), and `Matplotlib`, a 2D graphics package used for `Python` for publication-quality image generation across user interfaces and operating systems (Hunter 2007).

References

Adams, W. S. 1915, PASP, 27, 236
Adams, W. S. 1925, Proc. Natl. Acad. Sci., 11, 382
Allende Prieto, C., Cooper, A. P., Dey, A., et al. 2020, Res. Notes Am. Astron. Soc., 4, 188
Astropy Collaboration (Robitaille, T. P., et al.) 2013, A&A, 558, A33
Benítez, N., Dupke, R., Moles, M., et al. 2014, ArXiv e-prints [arXiv:1403.5237]
Bergeron, P., Dufour, P., Fontaine, G., et al. 2019, ApJ, 876, 67
Bertin, E., & Arnouts, S. 1996, A&AS, 117, 393
Bonoli, S., Marín-Franch, A., Varela, J., et al. 2021, A&A, 653, A31
Carrasco, J. M., Catalán, S., Jordi, C., et al. 2014, A&A, 565, A11
Cenarro, A. J., Moles, M., Marín-Franch, A., et al. 2014, in Observatory Operations: Strategies, Processes, and Systems V, Proc. SPIE, 9149, 91491I
Cenarro, A. J., Moles, M., Cristóbal-Hornillos, D., et al. 2019, A&A, 622, A176
Chiappini, C., Minchev, I., Starkenburg, E., et al. 2019, The Messenger, 175, 30
Cui, X.-Q., Zhao, Y.-H., Chu, Y.-Q., et al. 2012, Res. Astron. Astrophys., 12, 1197
Cukanovaite, E., Tremblay, P. E., Freytag, B., Ludwig, H. G., & Bergeron, P. 2018, MNRAS, 481, 1522
Cukanovaite, E., Tremblay, P. E., Freytag, B., et al. 2019, MNRAS, 490, 1010
Dalton, G., Trager, S. C., Abrams, D. C., et al. 2012, in Ground-based and Airborne Instrumentation for Astronomy IV, eds. I. S. McLean, S. K. Ramsay, & H. Takami, SPIE Conf. Ser., 8446, 84460P
De Angeli, F., Weiler, M., Montegriffo, P., et al. 2022, A&A, in press, https://doi.org/10.1051/0004-6361/202243680
Doherty, C. L., Gil-Pons, P., Siess, L., Lattanzio, J. C., & Lau, H. H. B. 2015, MNRAS, 446, 2599
Downes, R. A. 1986, ApJS, 61, 569
Dufour, P., Blouin, S., Coutu, S., et al. 2017, in 20th European White Dwarf Workshop, eds. P. E. Tremblay, B. Gaensicke, & T. Marsh, ASP Conf. Ser., 509, 3
Eisenstein, D. J., Liebert, J., Harris, H. C., et al. 2006, ApJS, 167, 40
Fantin, N. J., Côté, P., & McConnachie, A. W. 2020, ApJ, 900, 139
Fontaine, G., Brassard, P., & Bergeron, P. 2001, PASP, 113, 409
Fowler, R. H. 1926, MNRAS, 87, 114
Gaia Collaboration (Prusti, T., et al.) 2016, A&A, 595, A1
Gaia Collaboration (Brown, A. G. A., et al.) 2021a, A&A, 649, A1
Gaia Collaboration (Smart, R. L., et al.) 2021b, A&A, 649, A6
Gaia Collaboration (Montegriffo, P., et al.) 2022, A&A, in press, https://doi.org/10.1051/0004-6361/202243709
Gentile Fusillo, N. P., Gänsicke, B. T., & Greiss, S. 2015, MNRAS, 448, 2260
Gentile Fusillo, N. P., Tremblay, P.-E., Gänsicke, B. T., et al. 2019, MNRAS, 482, 4570
Gentile Fusillo, N. P., Tremblay, P.-E., Bohlin, R. C., Deustua, S. E., & Kalirai, J. S. 2020, MNRAS, 491, 3613
Gentile Fusillo, N. P., Tremblay, P. E., Cukanovaite, E., et al. 2021, MNRAS, 508, 3877
Green, R. F., Schmidt, M., & Liebert, J. 1986, ApJS, 61, 305
Green, G. M., Schlafly, E. F., Finkbeiner, D., et al. 2018, MNRAS, 478, 651
Harris, H. C., Munn, J. A., Kilic, M., et al. 2006, AJ, 131, 571
Hertzsprung, E. 1915, ApJ, 42, 111
Holberg, J. B. 2009, J. History Astron., 40, 137
Hollands, M. A., Koester, D., Alekseev, V., Herbert, E. L., & Gänsicke, B. T. 2017, MNRAS, 467, 4970
Hollands, M. A., Tremblay, P. E., Gänsicke, B. T., Gentile-Fusillo, N. P., & Toonen, S. 2018, MNRAS, 480, 3942
Hunter, J. D. 2007, Comput. Sci. Eng., 9, 90
Ibeling, D., & Heger, A. 2013, ApJ, 765, L43
Ivezic, Z., Tyson, J. A., Acosta, E., et al. 2019, ApJ, 873, 111
Jiménez-Esteban, F. M., Torres, S., Rebassa-Mansergas, A., et al. 2018, MNRAS, 480, 4505
Kepler, S. O., Pelisoli, I., Koester, D., et al. 2015, MNRAS, 446, 4078
Kepler, S. O., Pelisoli, I., Koester, D., et al. 2016, MNRAS, 455, 3413
Kepler, S. O., Pelisoli, I., Koester, D., et al. 2019, MNRAS, 486, 2169
Kilic, M., Bergeron, P., Kosakowski, A., et al. 2020, ApJ, 898, 84
Kleinman, S. J., Harris, H. C., Eisenstein, D. J., et al. 2004, ApJ, 607, 426
Kleinman, S. J., Kepler, S. O., Koester, D., et al. 2013, ApJS, 204, 5
Koester, D. 2010, Mem. Soc. Astron. It., 81, 921
Kollmeier, J. A., Zasowski, G., Rix, H. W., et al. 2017, ArXiv e-prints [arXiv:1711.03234]
Kondo, M., Noguchi, T., & Maehara, H. 1984, Ann. Tokyo Astron. Obs., 20, 130
Leggett, S. K., Bergeron, P., Subasavage, J. P., et al. 2018, ApJS, 239, 26
Lindegren, L., Bastian, U., Biermann, M., et al. 2021a, A&A, 649, A4
Lindegren, L., Klioner, S. A., Hernández, J., et al. 2021b, A&A, 649, A2
López-Sanjuan, C., Vázquez Ramió, H., Varela, J., et al. 2019, A&A, 622, A177
López-Sanjuan, C., Tremblay, P. E., Ederoclite, A., et al. 2022, A&A, 658, A79
Luyten, W. J. 1979, New Luyten Catalogue of Stars with Proper Motions Larger Than Two Tenths of an Arcsecond; and First Supplement; NLTT
Marín-Franch, A., Chueca, S., Moles, M., et al. 2012, in Modern Technologies in Space- and Ground-based Telescopes and Instrumentation II, eds. R. Navarro, C. R. Cunningham, & E. Prieto, SPIE Conf. Ser., 8450, 84503S
Marín-Franch, A., Taylor, K., Santoro, F. G., et al. 2017, in Highlights on Spanish Astrophysics IX, eds. S. Arribas, A. Alonso-Herrero, F. Figueras, C. Hernández-Monteagudo, A. Sánchez-Lavega, & S. Pérez-Hoyos, 670
McCleery, J., Tremblay, P.-E., Gentile Fusillo, N. P., et al. 2020, MNRAS, 499, 1890
McCook, G. P., & Sion, E. M. 1999, ApJS, 121, 1
Montegriffo, P., De Angeli, F., Andrae, R., et al. 2022, A&A, in press, https://doi.org/10.1051/0004-6361/202243880
Munn, J. A., Harris, H. C., von Hippel, T., et al. 2017, AJ, 153, 10
Noguchi, T., Maehara, H., & Kondo, M. 1980, Ann. Tokyo Astron. Obs., 18, 55
Oke, J. B., & Gunn, J. E. 1983, ApJ, 266, 713
Rolland, B., Bergeron, P., & Fontaine, G. 2018, ApJ, 857, 56
Rowell, N., & Hambly, N. C. 2011, MNRAS, 417, 93
Russell, H. N. 1914, Popular Astron., 22, 275
Sion, E. M., Greenstein, J. L., Landstreet, J. D., et al. 1983, ApJ, 269, 253
Taylor, K., Marín-Franch, A., Laporte, R., et al. 2014, JAI, 3, 50010
Tremblay, P. E., & Bergeron, P. 2009, ApJ, 696, 1755
Tremblay, P. E., Bergeron, P., & Gianninas, A. 2011, ApJ, 730, 128
Tremblay, P. E., Ludwig, H. G., Steffen, M., & Freytag, B. 2013, A&A, 559, A104
van Maanen, A. 1917, PASP, 29, 258
van Maanen, A. 1920, Contributions from the Mount Wilson Observatory/Carnegie Institution of Washington, 182, 1
Wenger, M., Ochsenbein, F., Egret, D., et al. 2000, A&AS, 143, 9
Wesemael, F., Greenstein, J. L., Liebert, J., et al. 1993, PASP, 105, 761
York, D. G., Adelman, J., Anderson, J. E., Jr, et al. 2000, AJ, 120, 1579